Specifications for a wide field of view fully sampled array of bolometers at the IRAM 30m telescope.

Samuel Leclercq. 2007 April 02, updated July 18.

Abstract.

IRAM wishes to build a new wide field of view bolometer array that would be capable of utilizing the full capacity of the 30m telescope. This goal would represent a significant improvement compared to the current instrument. This article presents the specifications for a fully sampled array of bolometers, in the 4 wavelengths bands available, filling the current and future field of view of the 30m, and reaching the ideal performance of photon noise limitation.

Wavelengths bands.

The choice of the instrument wavelengths bands is motivated by antenna and atmospheric constraints. The atmospheric windows available a large part of the year at the 30m telescope are 3 mm (100 GHz), 2mm (150 GHz) and 1mm (250 GHz). Few weeks per year, very good weather conditions make the 850 µm (350 GHz) band very attractive. Astronomical considerations may be taken into account in the choice of instrumental bands. Typical astronomical subjects in millimeter wavelengths continuum emissions are high redshift surveys, star forming regions, molecular and dust clouds, and cold bodies. The 1 and 2 mm bands are the natural choices for most of the observations with the 30m. Their simultaneous acquisition would be excellent for subjects like the Sunyaev-Zeldovich effect in ionized gas regions. The 850 µm band is particularly interesting for the observation of dusty regions and redshifted objects since they both emit more in this band than in the longer wavelengths, compensating somehow for the more critical weather conditions and mediocre aperture efficiency. Though the 3 mm band looks less attractive than the others, I included specifications for this band for information.

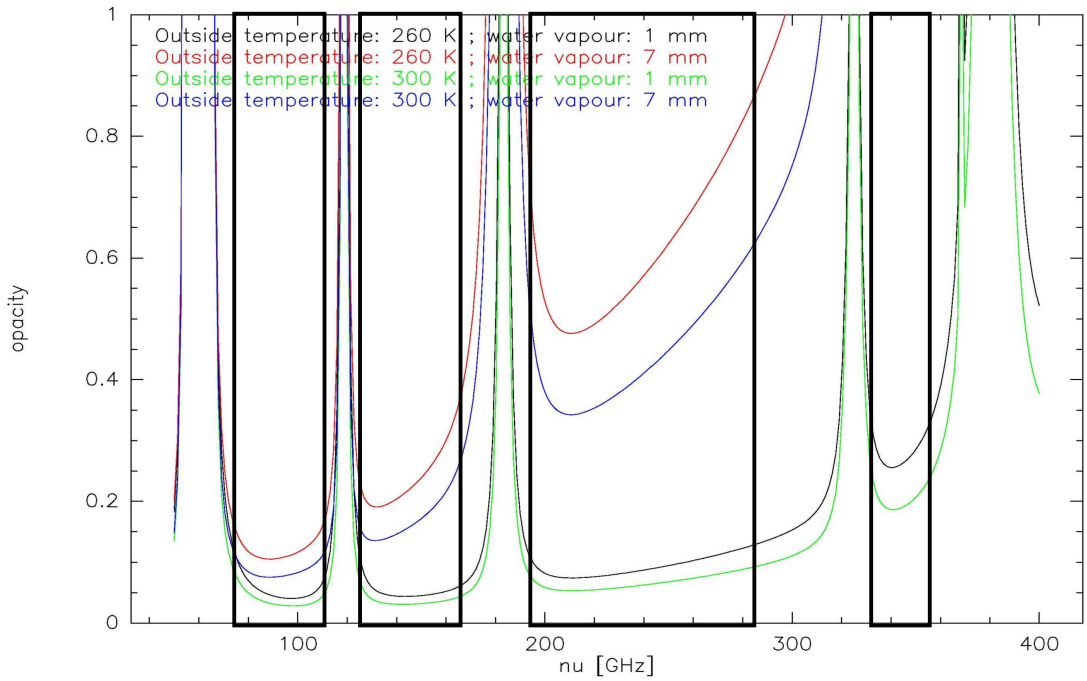

Fig. 1. Opacity model at Pico Veleta from ATM model, for winter (260K) and summer (300K) with good weather (1mm of water vapor) and bad weather (7mm). The 4 bands studied are the black rectangles: 94±18 GHz, 146±20 GHz, 240±45 GHz, 345±12 GHz.

As will be seen at the end of the NEP section, the signal to noise ratio increases as the square root of filters bandwidth, so at first order the bands should be as wide as possible. The best match with atmospheric constraints modeled from ATM model [1],[2], is shown in figure 1. Some legitimate reservations can be expressed about the maximization of the bandwidths. First, the bands extremes are very close to the atmospheric windows borders, so the filters must absolutely cut any power outside the bands; in the document we consider perfect rectangle functions for the filters (which seems reasonable according to recent filters profile [3]). Second, the little transition region between two bands may be constraining for a dichroic separating of the optical paths. Third, the very wide bandwidth of the 240 GHz windows may be too large for some sources and for power comparison with the 146 GHz band, it may also include too many astrophysical lines leading to sources confusion. Nevertheless, spectroscopy on these large bands could reverse these reservations.

Field of view and beam pattern.

The current filed of view (FOV) of the 30m is 4.4 arc minutes, limited by the Nasmyth mirror. With a new cabin optics design, an improvement between 10 and 12 arc minutes is studied [4] (a new secondary mirror and instrument position could increase the fov up to 20 arcmin [5]). Table 1 gives for each band the angular size of the full width half maximum (FWHM) diffraction pattern and the number of pixels needed to fully sample each FOV using 2 pixels per diffraction pattern diameter.

Table 1. Bolometer array geometrical characteristics, using pixels size of HWHM Airy disk. n_d is the number of pixels in the focal plane diameter (FOV) and N_d is the number of pixels covering the plane. The extra n_d in N_d formula insures the tilling fully covers the image.

Band	FWHM Airy disk (θ_a)	Number of pixels in FOV diameter: $n_d = FOV/(\theta_a/2)$			Number of pixels in FOV disk: $N_d \approx (\pi\, n_d^2/4) + n_d$		
		4.4' FOV	10' FOV	12' FOV	4.4' FOV	10' FOV	12' FOV
94 GHz 3.20 mm	22.6''	23	53	64	450	2300	3300
146 GHz 2.05 mm	14.5''	36	83	99	1100	5500	7900
240 GHz 1.25 mm	8.8''	60	136	163	2900	15000	21000
345 GHz 0.87 mm	6.2''	86	195	234	5900	31000	44000

A discussion of the relative merits of filled arrays, with instantaneous Nyquist sampling, and sparsely sampled arrays, with “fully efficient” horned pixels, lingers on in the bolometer community [6]. “Pro horns” argue that (1) the big number of pixels in a filled array leads to non-trivial increase in complexity, (2) the lower thermal background per pixel requires lower NEPs reach equivalent sensitivity at same operating temperatures, (3) the filled array has no intrinsic selectivity with regard to the acceptance angle and the beam definition has to be provided externally by a partly cold optical chain, involving bigger cryostats and IR filter problems [7]. These problems are real but technically surmountable, whereas the extra time and mapping method complexity can’t be avoided with horned arrays. So the horns versus filled arrays discussion leads to ponder the instrument price versus scanning time ratio. The subject of this document is not this discussion but the definition of the ideal instrument for the 30m, allowing the fastest, widest and simplest scanning scheme

with the lowest noise possible, which can only be achieved with filled arrays, assuming all their constraints can be overcome. Critical points for a fully sampled array are the pixel efficiency, which is proven now [8], and angular selectivity (through Lyot stops and filters), which still need to be proved at millimeter wavelength (for example the fight against stray lights was a major battle in the conception of SCUBA 2 [9],[10]).

The diffraction pattern considered in table 1 is the Airy diffraction pattern obtained with an aperture diameter D = 30m, hence a FWHM $\theta_a = 1.03\lambda/D$. In practice, the main parabola steepness, the secondary mirror closing, the surface deformation effects, and the effects of stops and tapers used for side lobes minimization, lead to wider and lower blobs. We kept the Airy pattern in the pixels size calculation for its simplicity and because over-sampling the center of the band is better for the high frequency part. Nevertheless, for correct photometric evaluations, notably sensitivity to point sources, one has to use a more realistic beam pattern. Based on antenna tolerance theory and in situ measurements it is possible to derive such a pattern; table 2 gives these empirical parameters for the 30m [11].

Table 2. Parameters for realistic expression of the 30m beam pattern.

Name	Symbol	Value
Aperture efficiency at long wavelengths	ε_0	0.63
Steepness reduction factor	R	0.8
Large-scale deformation correlation length	d_1	3 m
Panel frame misalignment correlation length	d_2	1.85 m
Panel deformations correlation length	d_3	0.45 m
Deformations rms-values (same for the 3 error beams)	σ_h	0.055 mm
Taper (Lyot stops) width coefficient	kt	1.1

Airy type beam pattern (I) and Gaussian tapered approximation (G) without error beams are:

$$I(r,\varphi) = \left(\frac{2\ J_1(r)}{r}\right)^2 \qquad G(r,\varphi) = \frac{2}{\sigma_G^2}\exp\left(\frac{-r^2}{2\sigma_G^2}\right) \qquad \sigma_G^2 = \frac{kt\ \ 1.616}{\sqrt{2\ln(2)}} \tag{1}$$

where r and φ are polar coordinates on the focal plane: $r = \pi\cdot\sin(\theta)\cdot D/\lambda$, θ is the angle between incident ray and optical axis, D is the telescope diameter, λ is the wavelength, and J_1 is the 1st order Bessel function.

The telescope realistic beam pattern (F) including gaussian error beams is characterized by the wavefront deformations (σ_φ), the error beams relative amplitude (q_e), and aperture efficiency (ε_a):

$$\sigma_\varphi(\nu) = R\,\frac{4\pi\nu}{c}\sigma_h \qquad q_e(\nu,i) = \frac{1}{\varepsilon_0}\left(\frac{d_i}{D}\right)^2\left(1-\exp\left(-\sigma_\varphi(\nu)^2\right)\right) \qquad \varepsilon_a(\nu) = \varepsilon_0\exp\left(-3\left(\sigma_\varphi(\nu)\right)^2\right)$$

$$F(r,\varphi,\nu,bp) = \exp\left(-3\left(\sigma_\varphi(\nu)\right)^2\right)bp(r,\varphi) + \sum_i q_e(\nu,i)\ \exp\left(-\left(\frac{r\,d_i}{2D}\right)^2\right) \tag{2}$$

where ν is the photons frequency and bp is the beam pattern without error beams (I or G). As illustrated in Figure 2, the shortest the wavelength is the strongest the aperture efficiency effect is. For instance at 1mm, 75% of the peak height is diluted into error beams !

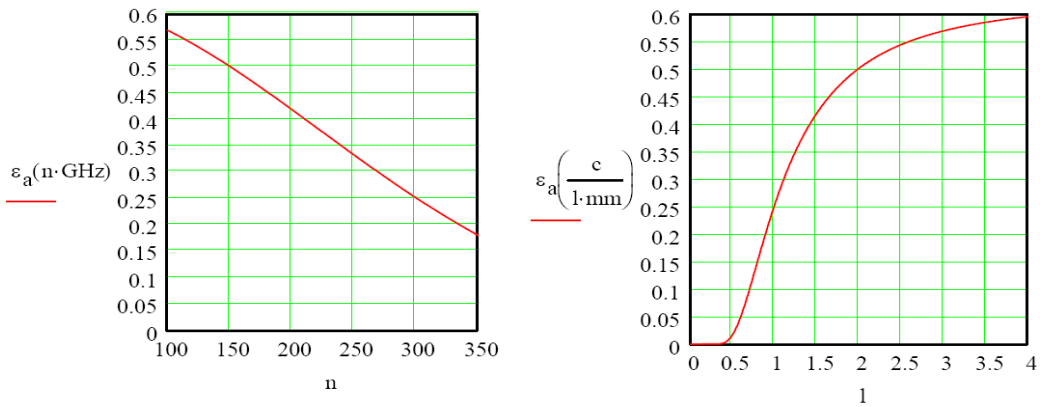

Figure 2: effect of the aperture efficiency as a function of frequency (n) or wavelength (l).

The relative power (or normalized luminosity) (L) contained in a disk is the integral of the diffraction pattern. For a circular pupil, the integration on the focal plane polar coordinate can be expressed analytically as a function of the number of pixels in the disk radius (n_r). The normalized luminosity for the Airy type pattern (L_a), Gaussian pattern (L_g), sum for the 3 error beams (L_e) and generalized beam (L_n) are:

$$L_a(n_r) = 1 - \left(J_0(r_{px} n_r)\right)^2 - \left(J_1(r_{px} n_r)\right)^2 \qquad L_g(n_r) = 1 - \exp\left(-\frac{1}{2}\left(\frac{r_{px} n_r}{\sigma_G}\right)^2\right)$$

$$L_e(n_r) = \sum_i 1 - \exp\left(-\left(\frac{r_{px} n_r}{2}\frac{d_i}{D}\right)^2\right)$$

$$L_N(\nu, sg) = \exp\left(-3\,\sigma_\varphi(\nu)^2\right)\frac{sg^2}{2} + \frac{3}{\varepsilon_0}\left(1 - \exp\left(-\,\sigma_\varphi(\nu)^2\right)\right)$$

$$L_n(r, \varphi, \nu, L_{bp}) = \frac{1}{L_N(\nu, sg)}\left(\exp\left(-3\,\sigma_\varphi(\nu)^2\right)\frac{sg^2}{2}L_{bp}(n_r, sg) + \frac{1}{\varepsilon_0}\left(1 - \exp\left(-\,\sigma_\varphi(\nu)^2\right)\right)L_e(n_r)\right) \tag{3}$$

where ν is the frequency, r_{px} is the size of a pixel in the focal plane, J_0 and J_1 are Bessel functions and sg is the "width" parameter of the main beam ($\sqrt{2}$ for the Airy pattern and σ_G for the Gaussian pattern). L_N is the value of the integration of the beam pattern F at infinite radius, corresponding to integration over the 2π steradian half plane in front of the aperture. The conservation of energy impose that the relative power is 1 at infinity, hence the $1/L_N$ factor in the general expression $L_n(r,\varphi,\nu,L_{bp})$. L_{bp} is either L_g or L_a depending on the choice to use a taper or not. Figure 3 shows the behavior of the relative power without and with error beams.

For photometric calculations, extended sources are viewed as emitting from 2π steradian, hence on each point of the focal plane all the beam patterns components from each point of a source are summed and the relative power is therefore always equal to one. But for a single point source there is only one diffraction pattern, and as Figure 3 illustrates, the influence of aperture efficiency and error beams is huge at small radius of integration, hence the importance of utilizing the realistic beam pattern for correct sensitivity predictions.

The normalized beam pattern is the derivative of the relative power:

$$F_n(n_r, \varphi, \nu, bp, sg) = \frac{F(n_r r_{px}, \varphi, \nu, bp)}{L_N(\nu, sg)} \tag{4}$$

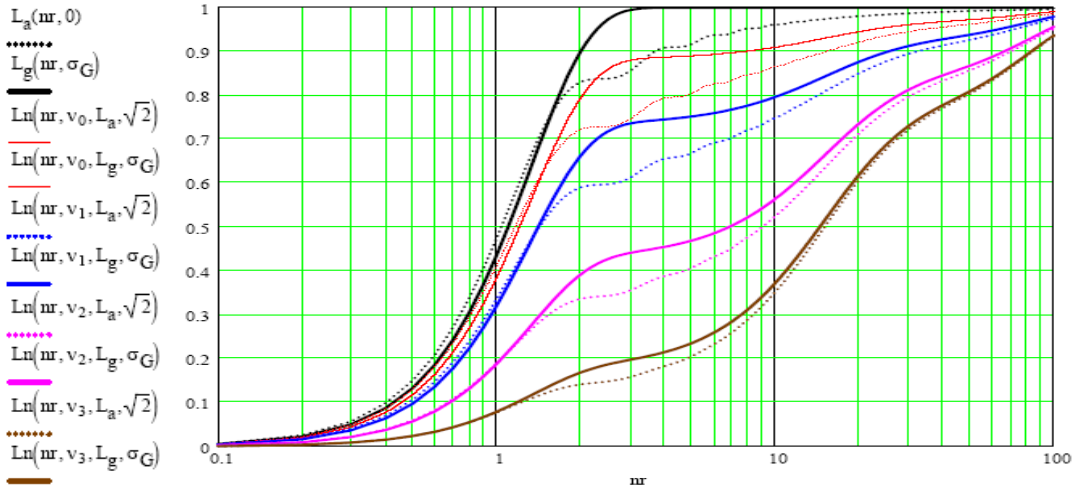

Figure 3. Relative power as a function of the number of pixels in a disk radius, for the Airy type pattern (L_a) (black dots), the tapered Gaussian pattern (L_g) (black solid) and the realistic beam pattern including error beams (Ln) with either the Airy pattern (dots) or the tapered Gaussian (solid) as the main beam. Red = 3.20 mm band, Blue = 2.05 mm band, Magenta = 1.25 mm band, Brown = 0.87 mm band.

The beam pattern of equation (4) do not take into account the spill-over effect, enabling sources behind the antenna to radiate on the focal plane, and respectively leading to losses of energy in side lobes behind the antenna from sources in front of it. Since the implementation of the spill-over effect in the antenna tolerance theory complicates the equations, a convenient numerical correction uses the forward efficiency F_{eff}. This empirical parameter gives the fraction of absorbed light from the half space in front of the telescope, deduced from sky dips measurements [12]. Photometric calculations have to use this corrected model since it adds the ground as an additional background source and it reduces the power from forward sources.

Remark: for an existing instrument it is generally not necessary to use the antenna tolerance theory. The concepts of antenna and brightness temperatures allow to calculate the power received by the system without knowing the details of the Fourier coverage of the aperture, and the consequences of the grading are mainly taken into account through 3 global factors: the aperture efficiency (ε_a), the beam efficiency (B_{eff}) and the forward efficiency (F_{eff}). As seen previously ε_a is the relative loss of intensity at the center of the beam, which is equivalent to a ratio of effective collecting area versus geometric area. The definition B_{eff} from [12] is

$$B_{eff} \equiv \frac{T_a'}{T_{mb}} = \varepsilon_a \frac{S\Omega_b}{\lambda^2} = 0.8899\ \varepsilon_a(\nu)\ kt^2 \qquad \Omega_b = 2\pi\int_0^\infty \exp\left(\frac{-r^2}{2\sigma_G^2}\right)\theta\, d\theta$$

where T_a' is the antenna temperature outside the atmosphere, T_{mb} is the main-beam brightness temperature, Ω_b is the solid angle of a rectangle function with the same height as the Gaussian beam pattern and containing the same energy. The generalization of B_{eff} to any beam pattern can be done with the generalization of Ω_b. Hence ε_a, B_{eff} and F_{eff} can respectively be interpreted as the efficiencies at center of the beam, in the main beam (Ω_b) and in the full beam (antenna FOV). Unfortunately B_{eff} presented in [12], calculated in [11], deduced from equation (4), and the empirical values in [11] and [12] disagree, with $\Delta B_{eff} \leq 0.3$, which is bad for the low value in the 0.87 mm band. Despite these inconsistencies it is better to use the "realistic" beam pattern model for point sources photometric calculations than disregarding the effect of error beams on the real beam.

Radiation power budget on a pixel.

The background sources always contributing to the power budget on the pixel are the atmosphere, the ground, the telescope and the optical chain. The power absorbed from these sources has to be compared to the power from typical astronomical sources such as the Cosmic Microwave Background (CMB), a 1K Rayleigh-Jeans extended source, a 1mJy punctual source, a 1000 Jy medium size source and Jupiter.

The photons are attenuated between the sources and the detector by the emissivity of the sources, the elevation angle (el), the transmissions of objects between source and detector, the spillover effect, and the detector efficiency. The opacity (τ), transmission (t) and emissivity (e) are related by $t = \exp(-\tau/\sin(el))$ and $e = 1-t$.
The calculations presented here used an elevation of 50° and a 4th order polynomial approximation cut by rectangle functions to simulate the atmosphere opacity. The errors are about 10% at the rectangles edges, and less than 1% elsewhere.
To fight stray lights in filled arrays and cut all frequencies outside the bands it is necessary to use a Lyot stop, cold baffles and several layers of filters at different temperature stages. Thermal blockers cut infra-red light (5 µm, 50 µm, etc.), edge filters delimitate more strictly the useful domain, and the band-pass filter may be preceded by dichroics and neutral density filters. The power budget presented below was calculated with a realistic configuration of 8 filters: 1 at 300 K, 2 at 77 K, 4 at 4 K and the band-pass filter at 300 mK. Each filter transmission was modeled by a simple rectangle function of height $t_f = 0.95$ [3], leading to similar errors than the atmosphere approximation.
Figure 4 shows the atmosphere and total filters transmissions used in the calculations.

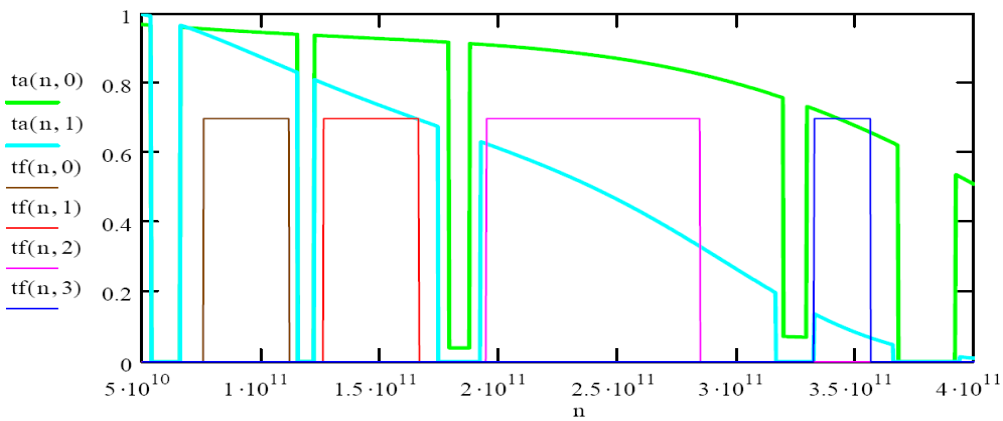

Figure 4. Transmissions (t) as a function of frequency (n). Atmospheric transmission (t_a) at 260K, 1 mm of water vapor in green, and 7 mm of water vapor in cyan. Filters transmission (t_f): 3.20 mm (94 GHz) band in brown, 2.05 mm (146 GHz) band in red, 1.25 mm (240 GHz) band in magenta, and 0.87 mm (345 GHz) in blue.

The ohmic losses are 1% per mirror [13] and are responsible for their emissivity. The term "spill-over" calculated below includes all the losses not contributing to the background and not due to the detectors efficiency. Since the forward efficiency includes all losses from telescope entrance to the mirror M6 (convention used in measurements at the 30m [13]), the optical system attenuations factors are:

Pixel efficiency: $\eta = 0.90$. Cold filters transmission: $t_f = t_{fbp} \cdot t_{f77} \cdot t_{f4} = 0.70$.

Mirrors reflection: $t_m = (1-0.01)^6$. Telescope + optics: $t_t = t_m \cdot t_{f300} = 0.89$.

Spill-over: $sp(\nu) = F_{eff}(\nu)/t_m \Rightarrow sp(94/146/240/350GHz)=0.98/0.97/0.90/0.80$

The attenuation factor formula for a given source is:

$$\mathrm{aet}(\nu) = \eta \cdot \mathrm{sp}(\nu) \cdot e_s(\nu) \cdot \prod_i t_i(\nu) \tag{5}$$

where ν is the frequency and t_i is the transmission of objects between the source and the detector. For the ground, sp(ν) has to be replaced with (1-sp(ν)) and the typical emissivity is $e_g = 0.3$ [14]. The aperture efficiency at long wavelength calculated with these attenuation factors is $\varepsilon 0 = \eta\ \mathrm{sp}(0)\ t_t\ t_f(\nu_c) = 0.55$.

The background sources (atmosphere, telescope and optics) and the CMB are continuum sources, which photon emission is described by the black body model. The Planck formula gives their brightness (B):

$$B(T,\nu) = \frac{2h}{p_o\, c^2} \frac{\nu^3}{\exp\left(\frac{h\nu}{kT}\right) - 1} \left[\frac{W}{m^2\, Hz \cdot sr}\right] \qquad B_{RJ}(T,\nu) = \frac{2kT\nu^2}{c^2} \qquad T_{RJ} = e_s(\nu) \frac{c^2}{2k\nu^2} B(T,\nu) \tag{6}$$

where h is the Planck constant, c is the speed of light, k is the Boltzmann constant, ν is the photons frequency, p_o is the polarization factor (p_o=1 for unpolarized light and p_o=2 with a polarizer) and RJ is the Rayleigh-Jeans approximation. The numbers in table 3, listing the powers deposited by background and reference sources, were calculated for unpolarized beam. Though polarized beams should be considered as an option of valuable astrophysical interest [15].

The multiplication of the brightness with attenuation factors, and integration on the pixel field of view and pupil (30m main mirror), gives the spectral power:

$$P_\nu(T,\nu) = U \cdot \mathrm{aet}(\nu) \cdot B(T,\nu) \quad [W/Hz] \tag{7}$$

where $U=S\Omega$ is the throughput (etendue) of the system ; $S=707m^2$ being the surface of the pupil and $\Omega=\pi(\theta_a/4)^2$ the solid angle with which a pixel sees the pupil.

The total power on a pixel is the integration on the frequency domain of the spectral power; between the filters boundaries ν_{min} to ν_{Max} for all the objects before the filters, over the whole frequency domain for the cold part after them:

$$P(T) = \int_{\nu_{min}}^{\nu_{Max}} P_\nu(T,\nu)\, d\nu \ \ [W] \qquad P_{cold} = ps^2 \sigma_S\, T_{cold}^4 \tag{8}$$

where σ_S is the Stefan constant and ps is the pixel size, which has to be larger than the wavelength to avoid an additional diffraction term, but as small as possible to minimize microfabrication costs; ps = 1.1 λ was chosen as a realistic value.

For a point source the beam pattern has to be considered. If the source flux is F [W/m^2/Hz], the power absorbed by a pixel is:

$$P_{pt}(F,n_r) = \frac{SF}{(2n_r)^2} \int_{\nu_{min}}^{\nu_{Max}} L_n(n_r,\nu) \cdot \mathrm{aet}(\nu) \cdot d\nu \tag{9}$$

The two extreme configurations are: $n_r = 0.5$ when the center of the diffraction blob is at the center of the pixel, and $n_r = 1$ when it is at the corner.

For intermediate angular sizes sources, the beam is the convolution of the source shape with the diffraction pattern, but for an angular diameter $\theta_s >> \theta_a$, a cylinder function can be used. For a source flux F_s, the power on a disk of n_r pixel in radius is:

$$P_s(F,n_r) = S\, F_s\, L_s \int_{\nu_{min}}^{\nu_{Max}} \mathrm{aet}(\nu)\, d\nu \qquad \text{where} \quad L_s = \left(\frac{n_r\, \theta_a}{\theta_s}\right)^2 \tag{10}$$

This expression was used in table 3 for the 50” diameter sources, covering disks of respectively 16, 38, 101, and 208 pixels for the 3.20, 2.05, 1.25, and 0.87 mm bands.

Table 3. Power budget on a pixel size of HWHM Airy disk, from background and reference sources. The second column gives the physical or black body temperatures of the sources. The power received by a pixel for each source in each band is given for good (bad) weather conditions. The Rayleigh-Jeans temperature below the power when relevant.

Source	T [K]	P [pW] for 1 (7) mm of water vapor (wv) T_{RJ} [K]			
		λ = 3.20 mm	λ = 2.05 mm	λ = 1.25 mm	λ = 0.87 mm
Atmosphere	260	**1.2 (2.6)** 13 (28) K_{RJ}	**1.8 (6.5)** 18 (65) K_{RJ}	**6.8 (27.6)** 30 (127) K_{RJ}	**3.8 (11.1)** 77 (227) K_{RJ}
Ground	260	0.2	0.3	1.8	0.9
Telescope + optics	280	**3.0** 29 K_{RJ}	**3.2** 29 K_{RJ}	**6.7** 29 K_{RJ}	**1.6** 29 K_{RJ}
77 K stage(1)	77	0.7	0.7	1.6	0.4
4 K stage(1)	4	0.05	0.03	0.04	≈ 0
0.3 K stage(1)	0.3	0.01	≈ 0	≈ 0	≈ 0
CMB (2)	2.725	0.090 (0.084) 1.07 K_{RJ}	0.052 (0.042) 0.58 K_{RJ}	0.031 (0.018) 0.17 K_{RJ}	0.001 (≈ 0) 0.04 K_{RJ}
Background total (P_{bkg})		**5.0 (6.5)**	**6.0 (10.8)**	**16.9 (37.7)**	**6.7 (13.9)**
1 K_{RJ} extended	n/a	0.085 (0.080)	0.092 (0.073)	0.181 (0.099)	0.034 (0.005)
1 mJy point center (3)	n/a	16 (15) $\times 10^{-6}$	14 (11) $\times 10^{-6}$	17 (10) $\times 10^{-6}$	1 (0) $\times 10^{-6}$
1 mJy point corner (3)	**n/a**	**13 (12) $\times 10^{-6}$**	**11 (9) $\times 10^{-6}$**	**14 (8) $\times 10^{-6}$**	**1 (0) $\times 10^{-6}$**
1000 Jy, 50” (4)	n/a	6.79 (6.39) 80 K_{RJ} ; 5 pixels	3.01 (2.41) 33 K_{RJ} ; 7 pixels	2.22 (1.25) 12 K_{RJ} ; 12 pixels	0.20 (0.03) 6 K_{RJ} ; 17 pixels
Jupiter (5), 50” (4)	150	12.6 (11.8) 148 K_{RJ} ; 5 pixels	13.4 (10.7) 147 K_{RJ} ; 7 pixels	26.1 (14.2) 144 K_{RJ} ; 12 pixels	4.8 (0.7) 142 K_{RJ} ; 17 pixels
Max power $P_{M=}P_{bkg}+P_{Jup}$		**17.7 (18.3)**	**19.4 (21.5)**	**42.9 (52.0)**	**11.5 (14.6)**
Dynamic 1mm wv: $P_{M(1)}/P_{1mJy(1)}$		1.4 $\times 10^6$	1.7 $\times 10^6$	3.2 $\times 10^6$	10.8 $\times 10^6$
Dynamic 7mm wv: $P_{M(7)}/P_{1mJy(7)}$		1.5 $\times 10^6$	2.3 $\times 10^6$	6.6 $\times 10^6$	94.1 $\times 10^6$
Dynamic bad on-off $(P_{M(7)}-P_{bkg(1)})/P_{1mJy(7)}$		1.1 $\times 10^6$	1.7 $\times 10^6$	4.5 $\times 10^6$	51.2 $\times 10^6$

(1) The emissivities of the cryostat temperature stages are calculated with the filters transmissions.
(2) The CMB is both an object of study and a background source.
(3) The maximum illumination from a point source stands between the center and the corner of a pixel.
(4) Angular diameter given in arc seconds, diameter on the array given in pixels after T_{RJ}.
(5) Jupiter flux depends on the band: 4500 Jy at 2.05 mm; 12000 Jy at 1.25 mm.

The background is always dominated by the optical chain during good weather and by the atmosphere during bad weather, except the 1.25 mm band always dominated by the atmosphere. The ratio of total maximum power versus smallest fluctuations to measure implies a bolometer linear response in a large range. On-off mode may allow a gain of an order of magnitude for homogeneous sky, but not that much in poor conditions (last line of the table). With variable pixels bias compensating the incident power it is possible to gain few more orders of magnitude on the dynamic.

Using B_{RJ} approximations, attenuation factors constant at the center of the band, and a pixel throughput $U = (\pi\lambda)^2/4^3$ obtained with $\theta_a \approx \lambda/D$, one can write a practical formula for quick estimations of the absorbed power:

$$P(T) = \frac{\pi^2}{4^3}\, aet(\nu_c)\; 2kT\; \Delta\nu \qquad (11)$$

For the atmosphere and telescope at 1mm water vapor, the calculation gives:

Band [mm (GHz)]	3.20 (94)	2.25 (146)	1.25 (240)	0.87 (350)
$P(T_{atm})$ [pW]	1.1	1.7	6.1	3.7
$P(T_{tel})$ [pW]	2.8	3.1	6.4	1.5

The error is reasonable with roughly 10% per component.

Noise Equivalent Power.

The fundamental limit of photon noise is expressed in terms of Noise Equivalent Power (NEP) (explanations on NEP definition and photon noise in [16]). The photon NEP has two components: a classical Poissonian shot noise and a bosons bunching noise [17]. The later is inversely proportional to the number of states (or modes) available at the detector surface $N_{modes} = 1/(\Delta_s \cdot \Delta_t)$, where Δ_s and Δ_t are the spatial and time coherence factors. Popular approximations are $1/\Delta_t = 1/(t_m \cdot \Delta\nu)$ (t_m is the measurement time) and $1/\Delta_s = U/\lambda^2$, valid only when $t_m >> \Delta\nu$ and $U >> \lambda^2$ [18]. for most cases the temporal condition is true, but the spatial condition is true only with incoherent beams, implying a detector much larger than a diffraction blob. The correct formulation of the spatial coherence factor for a point source and a square pixel is:

$$\Delta_s(r) = \frac{1}{(2r)^4}\int_{-r}^{+r}\int_{-r}^{+r}\int_{-r}^{+r}\int_{-r}^{+r} I(x-x', y-y')\, dx\, dy\, dx'\, dy' \qquad (12)$$

where I(x,y) is the diffraction pattern in Cartesian coordinates. This formula verifies $\Delta_s(r) = \lambda^2/U$ for totally incoherent beam and $\Delta_s(r) = 1$ for totally coherent beam. Using the Airy pattern instead of the real beam (F_n) induces negligible errors.

There is no analytical formulation for Δ_s and the numerical integration may be time consuming, so in practice an approximated formula is helpful. Thanks to fits on the real curve, I defined an approximation Δ_a verifying $|\Delta_a - \Delta_s| < 0.01$ everywhere. Expressed as a function of the number of FHWM blobs per pixel (n_{bp}) its formula is:

$$\Delta_a(n_{bp}) = \begin{cases} \exp\left(\ln(0.49)\cdot n_{bp}^{\;1.78}\right) & \text{if } n_{bp} \le 1 \\ 0.49\cdot\exp\left(\ln\left(\frac{0.015}{0.49}\right)\cdot\frac{n_{bp}^{\;0.1}-1}{10^{0.1}-1}\right) & \text{otherwise} \end{cases} \qquad (13)$$

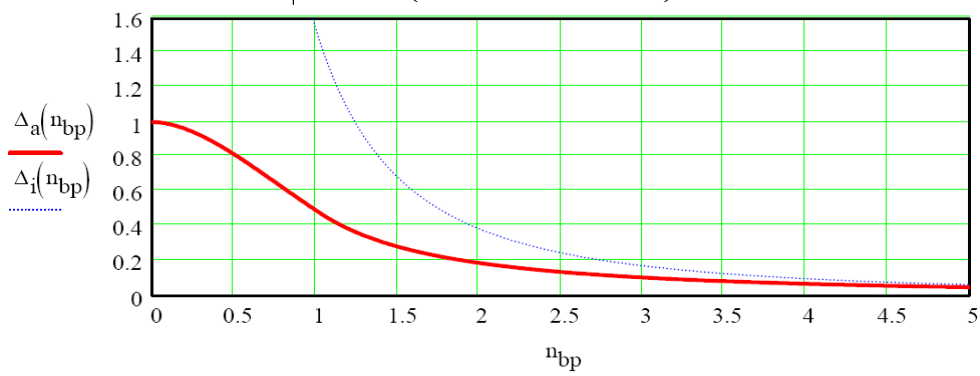

Figure 5. Spatial coherence factor of a point source illuminating a square pixel as a function of the number of FWHM Airy pattern in the pixel side (n_{bp} = 0.5 for 2 pixels in a FWHM). Δ_a is the fit to the real coherence factor, $\Delta_i = \lambda^2/D$ is the incoherent beam approximation.

Considering that the system bandwidth verifies the Nyquist criteria $\Delta f=1/2t_m$, the expression of the photon NEP is:

$$NEP^2 = \int_{\nu_{min}}^{\nu_{Max}} 2h\nu \frac{P_\nu(\nu)}{(\gamma(\nu))^2}\, d\nu + \int_{\nu_{min}}^{\nu_{Max}} p_o \cdot \Delta_a(n_{bp}(\nu)) \cdot \left(\frac{P_\nu(\nu)}{\gamma(\nu)}\right)^2 \cdot d\nu = NEP_p^2 + NEP_b^2 \tag{14}$$

NEP_p is the classical Poissonian component and NEP_b is the bosonic component. $n_{bp}(\nu) = \nu/(np\cdot\nu_c)$, where np = 2 is the number of pixels per FWHM diffraction pattern and ν_c is the center of the band. $\gamma(\nu)$ is the attenuation factor for the system power response: when $\gamma(\nu) = 1$ the formula gives the electrical NEP (at the pixel output), when $\gamma(\nu) \neq 1$ the formula gives the optical NEP (at the system input) [16]. For the bolometers specification it is interesting to calculate both the electrical NEP to impose a constraint on the bolometer intrinsic noise, and the optical NEP above the atmosphere, called Background Radiation Equivalent NEP (BNEP) [19], for quick estimations of the integration time to detect a given source. For the BNEP one has to use $\gamma(\nu) = \eta\cdot sp(\nu)\cdot t_a(\nu,\nu)\cdot t_t\cdot t_f(\nu)$ (see equation 5). Table 4 gives the contribution of the background sources to NEP and BNEP.

Table 4. Photon noise electrical NEP and optical BNEP for the ideal pixel at the 30m telescope. For each source the top number is the Poissonian NEP and the bottom number is the bosonic NEP. The numbers are given for a good (bad) atmosphere and non-polarized beam. All the values are above 0, but some are lower than the precision shown in the table.

Source	NEP_p and NEP_b [10^{-17}W/$\sqrt{Hz}$] at 1 (7) mm of water vapor							
	NEP				BNEP			
band	3.20mm	2.05mm	1.25mm	0.87mm	3.20mm	2.05mm	1.25mm	0.87mm
Atmosphere	**1.3** (1.9) **0.6** (1.4)	**1.9** (3.6) **0.8** (3.0)	**4.7** (9.5) **2.1** (8.7)	**4.2** (7.1) **2.2** (6.4)	2 (4) 1 (3)	4 (9) 2 (8)	11 (44) 5 (42)	13(170) 7 (154)
Ground	0.5 0.1	0.7 0.1	2.4 0.6	2.0 0.5	1 (1) 0 (0)	1 (2) 0 (0)	6 (12) 1 (3)	7 (49) 2 (13)
Telescope + optics	**1.9** **1.4**	**2.5** **1.5**	**4.7** **2.0**	**2.7** **0.9**	4 (4) 3 (3)	5 (6) 3 (4)	11 (21) 5 (9)	9 (64) 3 (22)
77 K stage	0.9 0.3	1.2 0.3	2.3 0.5	1.4 0.2	2 (2) 1 (1)	2 (3) 1 (1)	5 (10) 1 (2)	4 (33) 1 (6)
4 K stage	0.2 0.0	0.3 0.0	0.3 0.0	0.1 0.0	n/a	n/a	n/a	n/a
CMB	0.3 (0.3) 0.0 (0.0)	0.3 (0.3) 0.0 (0.0)	0.3 (0.2) 0.0 (0.0)	0.1 (0.0) 0.0 (0.0)	1 (1) 0 (0)	1 (1) 0 (0)	1 (1) 0 (0)	0 (1) 0 (0)
Photon Total	**2.6** (2.9) **1.6** (2.0)	**3.5** (4.6) **1.7** (3.4)	**7.5** (11) **3.0** (9)	**5.5** (8.0) **2.5** (6.5)	5 (6) 3 (4)	7 (12) 3 (9)	17 (52) 7 (43)	18(190) 9 (157)
Pixel goal = Total(1mm)/3	**1.0**	**1.3**	**2.7**	**2.0**	1.9	2.6	6.2	6.5
TOTAL	**3.2** (3.7)	**4.1** (5.9)	**8.5** (15)	**6.4** (11)	6 (8)	8 (15)	20 (67)	21(247)

The constraint on the pixel noise includes the complete reading chain (pixel intrinsic noise, multiplexing, amplification and digitization). The numbers calculated are ambitious but reachable with the techniques currently emerging.

With the assumption of narrow bandwidth filters and either negligible photon bunching (NEP_b=0) or totally incoherent beam ($\Delta_s\cdot P_\nu \approx (\lambda^2/U)\cdot(U\ aet\ B) \approx 2k\cdot aet\cdot T$), one can write a practical formula for quick estimations of the photon NEP:

$$NEP_p^2 = 2h\nu_c P(T) \qquad NEP_b^2 = aet(\nu)\cdot 2k\,T\cdot P(T) \tag{15}$$

Considering the atmosphere and telescope as the main photon noise sources and using the same approximations as equation 11, the NEP estimation at 1mm water vapor is:

Band [mm (GHz)]	3.20 (94)	2.25 (146)	1.25 (240)	0.87 (350)
$NEP_p(T_{atm})$ [$10^{-17}W/\sqrt{Hz}$]	1.6	2.4	6.1	6.0
$NEP_b(T_{atm})$ [$10^{-17}W/\sqrt{Hz}$]	2.0	2.9	7.1	8.9
$NEP_p(T_{tel})$ [$10^{-17}W/\sqrt{Hz}$]	2.4	3.1	5.9	3.7
$NEP_b(T_{tel})$ [$10^{-17}W/\sqrt{Hz}$]	4.7	5.0	7.2	3.5

The error is about 25% for NEP_p and a bit more than 200% for NEP_b. This can be considered as correct to estimate the order of magnitude of the noise. The over-estimation of NEP_b is mainly due to the use of $\Delta_i=\lambda^2/U=6.5$ instead of $\Delta_a=0.8$.

The approximation formula for both the total power and the equivalent noise don't create big errors, so the most delicate work in these specifications are not the precision of the calculations, but the good understanding and numbering of the background sources and attenuation factors.

From P and NEP formula one gets $P \sim \Delta\nu$ and that $NEP^2 \sim \nu\,\Delta\nu$, therefore the signal to noise depend on the filters bandwidth as $S/N \sim \sqrt{\Delta\nu}$. Thus the broadest bandwidths are the more attractive (astrophysical lines such as the 240 GHz CO lines, potentially annoying for some observations, are 2nd order considerations [20]).

The numbers in tables 3 and 4 are given for unpolarized beams. With 2 polarizations a factor 1/2 appears in the expression of the absorbed power, and a factor $1/\sqrt{2}$ appears in the expression of the NEP, leading to a more ambitious instrumental noise.

NET, NEFD and integration time.

The absorbed power depends on the coupling between telescope and detector. To describe the detector intrinsic performance it is helpful to use the *flux density*, which is independent on the telescope surface. The usual flux unit in radio astronomy is the Jansky: $1Jy = 10^{-26}\,W/m^2/Hz$. The Noise Equivalent Flux Density (NEFD) is defined as the level of flux density required to obtain a unity signal to noise ratio in one second of integration with the detector. The general expression for the NEFD of a detector with a spectral width $\Delta\nu$ and a collecting surface S is:

$$NEFD = \frac{o_m\,NEP}{S\int_{\Delta\nu}\gamma_x d\nu} \approx o_m\,\frac{NEP(\gamma_x)}{S\,\Delta\nu} \qquad \left[\frac{Jy}{\sqrt{Hz}}\right] \tag{16}$$

where o_m is the observing mode factor and γ_x an attenuation factor specifying the location at which the NEFD is calculated [16]. The notation $NEP(\gamma_x)$ means that $\gamma_x\gamma$ must be use in equation (14). The NEFD is mainly calculated outside the atmosphere, so using $NEP(\gamma_x)$ = BNEP simplifies the calculation, but this approximation is valid only if γ_x depends little on ν in $\Delta\nu$. For a continuous observing mode $o_m=1$. For On–Off observing mode the NEFD is increased by $\sqrt{2}$ because of the quadratic sum of the noise from 2 images, and if only half of the time is spent on the source it is increased by another factor $\sqrt{2}$, so that $o_m = 2$ as in [19].

The flux of a source is often expressed in terms of Rayleigh-Jeans temperature. In that case it is convenient to express the noise in terms of Noise Equivalent Temperature (NET):

$$NET = NEP\,\frac{1[K]}{P_{RJ}(1K)[W]} \tag{17}$$

Since $NEP\sqrt{\Delta f} = P_{noise}$ and $\Delta f = 1/2t_m$, the integration time t_σ necessary to detect a source with a signal to noise ratio σ is calculated from the NEP, or NEFD or NET as:

$$t_\sigma(P_s) = \frac{1}{2}\left(\sigma\frac{NEP}{P_s}\right)^2 \qquad t_\sigma(F_s) = \frac{1}{2}\left(\sigma\frac{NEFD}{F_s}\right)^2 \qquad t_\sigma(T_s) = \frac{1}{2}\left(\sigma\frac{NET}{T_s}\right)^2 \qquad (18)$$

To get rid of the factor ½ in the formula, an astrophysicist trick consists of including it in the noise definitions, and indicates this choice using seconds in the units:

$$NEFD\left[Jy\cdot\sqrt{s}\right] = \frac{NEFD\left[Jy/\sqrt{Hz}\right]}{\sqrt{2}} \qquad NET\left[K\cdot\sqrt{s}\right] = \frac{NET\left[K/\sqrt{Hz}\right]}{\sqrt{2}} \qquad (19)$$

The values of t_σ calculated with the noise term above the atmosphere (BNEP) are 10 to 30 % higher than calculated with the noise term at the detector (NEP). With BNEP the frequency dependent transmissions are averaged on the filter bandwidth, which does not reflect the exact effect of the atmosphere on "astrophysical" photons.

Table 5 gives the ideal pixel sensitivity in terms of equivalent noise, integration time at a given flux level, and minimum flux detected after a given integration time. Integration time and minimum flux are both calculated for a 3σ signal to noise ratio.

Table 5. Pixel sensitivity in terms of NEFD, NET, integration time to detect a 1mJy source at 3σ, and flux detection limit at 3σ in 1 hour. The integration time is a continuous observation of the source. This "snap-shot" mode supposes negligible sky noise and background rejection in the data processing; On-Off would takes 4× longer. The time is calculated for the 2 extreme cases where the center of the source is either at the center of a pixel or at the corner (which represent an actual sensitivity per pixel less than a mJy). The pixel angular coverage, total background powers, wished instrumental NEPs and total NEPs are recalled for information.

Parameter	Value in each band for 1 (7) mm of water vapor			
	3.20 mm 94 GHz	2.05 mm 146 GHz	1.25 mm 240 GHz	0.87 mm 345 GHz
Pixel coverage [arc sec]	11.3	7.3	4.4	3.1
P_{bkg} [pW]	5.0 (6.5)	6.0 (10.8)	16.9 (37.7)	6.7 (13.9)
NEP_{int} [$10^{-17}W/\sqrt{Hz}$]	1.0	1.3	2.7	2.0
NEP_{TOT} [$10^{-17}W/\sqrt{Hz}$]	3.2 (3.7)	4.1 (5.9)	8.5 (15)	6.4 (11)
NEFD [mJy·$\sqrt{s}$]	0.17 (0.21)	0.20 (0.36)	0.21 (0.64)	0.85 (9.64)
NET [μK·$\sqrt{s}$]	263 (326)	315 (568)	337 (1159)	1342 (16130)
t(1mJy,3σ) center [min]	**0.3 (0.5)**	**0.6 (2.0)**	**2.0 (17.2)**	**184 (2×10^4)**
t(1mJy,3σ) corner [min]	**0.5 (0.7)**	**1.0 (3.0)**	**2.9 (25.7)**	**273 (3×10^4)**
F(1hr,3σ) [mJy]	0.09 (0.11)	0.13 (0.23)	0.22 (0.66)	2.1 (24)

Filled arrays approaching the ambitious performances of table 5 are currently tested ([10], [21] and others). A precise comparison with existing instrument is difficult because it is related to the filled array versus feed horns discussion, where respective performances depend on many factors (observed objects, sky conditions, observing mode, data processing). But to give a feeling of the improvement the ideal bolometer array would represent compared to current instrument, table 6 displays a comparison between MAMBO 2 [7] and an optimal filled array with pixel angular acceptances 2.5 times larger than the ideal pixel in previous tables. This effective pixel angular size ($\theta = 4\lambda/\pi D$) is chosen to match the MAMBO 2 pixel size, defined as the half power beam width (HPBW) of the feed horn plus telescope diffraction pattern [22]. The coupling of the effective pixel with the 30m presents a beam throughput $U = \lambda^2$ (a standard value sometimes used in literature for instrument comparison [15]).

Table 6. MAMBO 2 and ideal effective pixel sensitivities. MAMBO 2 parameters are from [22] and its integration times are calculated with the IRAM time estimator web tool [23]. For the effective pixel, the times correspond to the detection of a 1mJy point source at 3σ level with the center of the diffraction pattern either at the center of the pixel or at the corner. OnOff mode supposes half of the time spent on the source and half of the time on a reference. Mapping mode supposes On The Fly observation for MAMBO 2, and a "snap-shot" for the effective pixel array (all the time on the source, assuming no sky noise and no stray light).

Parameter	MAMBO 2, 1.20 mm 2 mm wv		Ideal effective pixel, 1.25 mm 1 (7) mm wv	
	sky noise reduction	no sky noise reduction	source max pixel center	source max pixel corner
Pixel coverage ["]	11 (HPBW)		11 (=4λ /πD)	
Spacin between pixel ["]	20		~ 0	
P_{bkg} [pW]	n/a		103 (231)	
NEP_{int} [10^{-17}W/$\sqrt{Hz}$]	n/a		7.4	
NEP_{TOT} [10^{-17}W/$\sqrt{Hz}$]	n/a		23 (46)	
NEFD OnOff [mJy·$\sqrt{s}$]	40		1.2 (4.1)	
NEFD mapping [mJy·$\sqrt{s}$]	45 (On The Fly)		0.6 (2.0) (snap-shot)	
t(1mJy) OnOff [min]	60	204	3.1 (36)	17 (201)
t(1mJy) mapping 260"×260" [min]	820	3200	0.8 (9)	4.4 (50)

Tables 6 and 5 give an idea of the huge margin of progress available at the 30m. The theoretical "snap-shot" mode though, supposes no additional background and noise; in particular neither stray light nor sky noise (atmospheric turbulences). The sky noise can roughly be modeled as a 1/f noise, a systematic that can't be reduced with integration time. Its cut-off frequency is not well defined in the radio range, but experimental data suggest that the signal bandwidth could be shifted above the sky noise thanks to an image sampling rate around 120 Hz [20], implying a very fast electronic capable of sampling the pixels at several kHz. Even with the sky noise and stray lights problems addressed correctly, other factors depending on observed objects may reduce the gap between MAMBO 2 and a real optimal filled array [6].

The comparison of table 5 with table 6 shows that the detection time is shorter and more homogenous for small pixels than big pixels (which is another advantage than the gain in resolution), at the price of a more ambitious intrinsic noise to beat the photon noise. This is due to a better ratio of point source energy versus background energy (small pixels covers only the maximum of the diffraction blob), and a smaller difference between neighbor pixels implying smaller time difference between blob maximum at the center of a pixel or at corner.

The information of the instrumental field of view (FOV) and filling factor are as important as the pixel sensitivity to give a real sense of the instrument performance. Indeed, mapping a 8×8 arcmin^2 FOV would take more than twice the time given in table 5 with an ideal instrument using the current optics of the 30m, but bigger FOV could be mapped with the same time as table 5 thanks to bigger instruments coupled to a new wider optical system covering at least 10 arc minutes in diameter. Hence, **the ideal instrument sensitivity on the 30m telescope with updated optics is 1 mJy at 3σ in 0.3, 0.6, 2.0, and 284 minutes for respectively 3.2, 2.05, 1.25 and 0.87 mm bands on a 12^2 arcmin^2 FOV**.

References.

[1] J.Cernicharo et al. *Atmospheric Transmission at Microwaves (ATM): An Improved Model for Millimeter/Submillimeter Applications*. EEE TRANSACTIONS ON ANTENNAS AND PROPAGATION, VOL. 49, NO. 12, DECEMBER 2001.

[2] ASTRO part in Gildas documentation. http://www.iram.fr/IRAMFR/GILDAS/

[3] M.Carter. Private discussion, based on recent filters profiles from Cardiff group.

[4] S.Leclercq. *New cabin mirrors for the 30m*. IRAM internal documentation (2007).

[5] IRAM internal workshop on future optics of 30m telescope (2006).

[6] Griffin, Bock, Gear. Applied Optics, 41, 6543, 2002.

[7] http://www.astro.uni-bonn.de/~bertoldi/projects/mambo/

[8] Private discussion with J.Staghun about efficiency of the future GISMO proptotype.

[9] Private discussion with W.Holland and P.Ade.

[10] W.Holland et al, *SCUBA 2: a 10,000 pixel submillimeter camera for the James Clerk Maxwell Telescope*.

[11] A.Greve et al. *The beam pattern of the IRAM 30-m telescope*. Astron. Astrophys. Suppl. Ser. 133, 271-284 (1998).

[12] D.Downes. *Radio Astronomy Techniques*. (1989).

[13] C.Thum. Private discussion.

[14] ground emissivity at mm wavelength … reference lost…

[15] F.X.Desert. Private discussion.

[16] S.Leclercq. *Discussion about Noise Equivalent Power and its use for photon noise calculation*. IRAM internal notes (2007).

[17] R. Hanbury Brown and R. Q. Twiss. *Interferometry of the intensity fluctuations in light. I. Basic theory: the correlation between photons in coherent beams of radiation*. Proc of the Royal Society of London A 242: 300-324 (1957).

[18] J.M.Lamarre. *Photon noise in photometric instruments at far-infrared and submillimeter wavelengths*. Applied optics, Vol 25, No. 6 (1986).

[19] D.Benford et al. *Noise equivalent power of background limited thermal detectors at submillimeter wavelengths*. International Jopurnal of Infrared Millimeter Waves, Vol. 19, No.7, 1998.

[20] R.Zylka. Private discussion.

[21] D.Benford et al, *Thousan-element multiplexed superconducting bolometer arrays*.

[22] http://www.iram.fr/GENERAL/calls/w07/w07/node18.html

[23] http://www.iram.es/IRAMES/obstime/obstab_bolo.html